Universität Hamburg

Master Thesis

The impact of Deep Convection on Overturning in the Labrador Sea

Katja Schultz

MSc. Ocean and Climate Physics
Universität Hamburg
Institut für Meereskunde
Experimentale Oceanography
Matr.-Nr.: 7041407

First Supervisor: Prof. Eleanor Frajka-Williams, Universität Hamburg
Second Supervisor: Dr. Louis Clément, National Oceanography Centre, UK

Abstract

This thesis investigates the variability of the local overturning circulation in the Labrador Sea over the past two decades, focusing on the influence of deep convection. Deep convection plays a crucial role in the ocean by facilitating the formation of Labrador Sea Water, significantly contributing to deep ocean ventilation and potentially impacting the meridional overturning circulation both locally and across the Atlantic. Utilizing Argo float data and optimal interpolation, I construct seasonal and decadal composites to analyze the impact of deep convection on local overturning at the AR7W line across the central Labrador Sea. My analysis reveals that strong deep convection years are associated with more vigorous overturning, especially in spring, where maximum transports of 3.7 Sv attributed to the formation of Labrador Sea Water occur, centered at 27.73 kgm^{-3}. In depth space, the most substantial overturning of 1.7 Sv occurs in winter, potentially driven by sinking in the boundary current, although this is not consistently linked to convection intensity. The results also suggest a decadal variability in winter convection, indicating that overturning strength fluctuates over longer time scales due to other processes. These findings emphasize the crucial role of deep convection in local overturning dynamics and underscore the necessity for long-term observational datasets to enhance our understanding of deep convection and its future impacts.

Contents

1
Introduction

The Labrador Sea, an arm of the North Atlantic Ocean between the Labrador Peninsula and Greenland, plays a crucial role in the global climate system as one of the few regions in the ocean where deep convection occurs in open waters. The Labrador Sea is a semi-enclosed basin featuring narrow, fast-moving boundary currents advecting heat and freshwater around the basin and a large, predominantly calm interior in the center (e.g. Straneo, 2006a).

During Winter, the cold atmosphere induces significant buoyancy loss at the ocean surface, mainly in the central basin, triggering deep convection and resulting in the formation of Labrador Sea Water (LSW) (Marshall and Schott, 1999; Pickart et al., 2002; Yashayaev et al., 2007). Deep convection in the Labrador Sea is characterized by high variability, driven by the interplay of multiple factors such as atmospheric conditions, oceanic preconditioning, and the presence of sea ice (Våge et al., 2009; Yashayaev, 2024; Yashayaev and Loder, 2016). These factors collectively influence the strength of convection, resulting in variable deep mixed layer depths up to 2500 m and differing properties of LSW.

As a major intermediate-depth water mass in the North Atlantic, LSW is crucial for ocean circulation and climate processes (Lazier et al., 2002; Marshall and Schott, 1999). After formation, LSW spreads across the North Atlantic through various pathways, including southward along the western boundary, eastward into the Irminger and Iceland basins, and even reaching subtropical latitudes (Chomiak et al., 2023; Straneo et al., 2003; Talley and McCartney, 1982; van Sebille et al., 2011; Yashayaev et al., 2007; Zou and Lozier, 2016). This cold fresh water mass is rich in oxygen and carbon dioxide, thus consequently ventilating the deep ocean when spread at depths (Rhein et al., 2002; Yashayaev et al., 2007).

Traditionally, LSW formation has been thought to play a significant role in driving the lower limb of the Atlantic Meridional Overturning Circulation (AMOC) (Le Bras, 2023; Yashayaev, 2024). The densification due to the mixing of cold surface water with deeper layers generates meridional density gradients and enhances sinking in the boundary currents encircling the basin (Straneo, 2006b). Both may be linked to the meridional overturning. Thus, years of strong deep convection with deep mixed layers and the formation of dense LSW should lead to strong local overturning in the Labrador Sea and possibly impact the overturning in the Atlantic. With ongoing climate change, surface layers will warm, and freshwater export from the Arctic will increase (Böning et al., 2016), potentially reducing the occurrence and strength of winter deep convection due to an increase in buoyancy. Presuming a solid link to overturning variability, the cessation of deep water formation may lead to a future decline in the AMOC and has been suggested to represent a tipping point (Drijfhout et al., 2015).

While there is consensus among models about the connection between AMOC variability and the intensity of deep winter convection (e.g. Böning et al., 2006; Böning et al., 2023;

S. G. Yeager and Danabasoglu, 2012; S. Yeager et al., 2021), recent observational studies of the Overturning in the Subpolar North Atlantic Program (OSNAP) have challenged this view. The OSNAP array is designed to observe the overturning in the subpolar North Atlantic, crossing the Labrador Sea in the west (OSNAP West) and spanning from Greenland to Scotland in the east (OSNAP East). The recent outcomes indicate a weak contribution of the Labrador Sea to subpolar overturning, despite periods of intense LSW formation in 2014 - 2018 (Li et al., 2021; Lozier et al., 2019). However, they only report the transport at densities of maximum overturning along the measuring array. Through examining the flow below 27.65 $kg\,m^{-3}$, the mean isopycnal of maximum overturning, Le Bras (2023) showed that the contribution of the Labrador Sea becomes more evident, with the lower limb transport increasing by over 2 Sv (1 $Sv \equiv 10^6\,m^3\,s^{-1}$). This results in a notable convergence of water masses into the dense LSW class, contributing 4.7 Sv of southward transport across the full OSNAP array, compared to only 0.1 Sv across OSNAP East.

Furthermore, LSW is partly advected to the south via the Deep Western Boundary Current, inducing AMOC variability further south on interannual to decadal time scales (Desbruyères et al., 2019; Jackson et al., 2016; Le Bras et al., 2023). To other parts, LSW recirculates in the subpolar North Atlantic, including OSNAP East, highlighting the role of water mass formation and deep convection in the Labrador Sea for the whole Atlantic basin. Therefore, it is crucial to gather long-term observations to understand better the contribution of Labrador Sea convection to the overturning in the Atlantic and allow for more robust predictions of the effects of climate change.

So far, observational and modeling studies have found notable inconsistencies in estimating the mean local overturning, with values ranging between 1 and 7 Sv, for different periods with various convection states (Böning et al., 1996; Delworth et al., 1993; Pickart and Spall, 2007; Rhein et al., 2002; Talley et al., 2003; Yashayaev and Loder, 2016). Holte and Straneo (2017) revealed a substantial seasonal signal above relatively limited mean overturning of 0.9 Sv. Since the seasonality has not been accounted for in the past, this might explain some of the inconsistencies. However, a comprehensive approach to address decadal variability and convection intensity must still be included.

In this thesis, I aim to examine the variability of local overturning in the Labrador Sea over the last two decades. Additionally, I want to test the hypothesis that local overturning in the Labrador Sea is more vigorous in years of strong deep convection, characterized by deep mixed layers and the formation of dense LSW.

The observation period of OSNAP has to be longer to capture decadal variability. Another approach is needed to resolve interannual to decadal changes in local overturning. I, therefore, utilize Argo floats to derive temperature and salinity sections of the AR7W line in the central Labrador Sea. Argo floats provide broad data coverage in time and space, enabling me to estimate seasonal composites on a decadal basis. The AR7W line is a repeated hydrographic section crossing the basin at the center of the deep convection site where the deepest mixed layers usually occur. Therefore, the section captures most of the overturning and LSW formation processes, unlike OSNAP West, which is located more to the east at the exit of the Labrador Sea. By using optimal interpolation, I derive composite sections to calculate the overturning in the decades 2004-2013 and 2024-2023 and of composites of strong and weak convection years.

The thesis is organized as follows: Chapter 2 provides further theoretical background, and chapter 3 describes the data and method for estimating the overturning. In chapter 4, I

present the seasonal estimates of the two decades and convection composites, and I asses the methodology. In the end, I discuss my results and give a conclusion in chapter 5 and 6.

2

Theoretical Background

The strength of the overturning circulation can be estimated by considering the volume transport across a section of the ocean. The transport is derived from the meridional absolute geostrophic velocity, v, which can be calculated from density data by using the thermal wind balance:

$$f_0 \frac{\partial v}{\partial z} = -\frac{g}{\rho_0} \frac{\partial \rho\prime}{\partial x}, \tag{2.1}$$

with f_0, the Coriolis parameter, g, the acceleration due to gravity, a background density ρ_0 and the perturbation density $\rho\prime$. Integrating eq. 2.1 yields the absolute geostrophic velocity as the sum of the relative geostrophic velocity, v_{rel}, and a constant, v_0:

$$v = \underbrace{-\frac{g}{f_0 \, \rho_0} \int \frac{d\rho\prime}{dx} \, dz}_{:= \, v_{rel}} + v_0. \tag{2.2}$$

v_{rel} can be directly calculated between density profiles along the section, derived from salinity and temperature. The constant velocity, v_0, can be derived with the help of direct measurements at a known depth or pressure level. In my case, I use Argo velocities at 1000 $decibar$ pressure level as the reference velocity, v_{ref}:

$$v_0 = v_{ref} \bigg|_{p \, = \, 1000 \, \text{decibar}} - v_{rel} \bigg|_{p \, = \, 1000 \, \text{decibar}}. \tag{2.3}$$

By zonally averaging the geostrophic velocity section, I estimate the overturning circulation strength in depth space, equivalent to Holte and Straneo (2017). This approach of obtaining the overturning was introduced by Fanning and Weaver (1997) and has also been employed on hydrographic data by Pickart and Spall (2007). The geostrophic velocity v is decomposed into the zonal average and a deviation velocity $v\prime$:

$$v(x, z) = \overline{v(z)}^x + v\prime(x, z). \tag{2.4}$$

$\overline{v(z)}^x$, is the overturning field, which is then multiplied by the length of the section, L, and cumulatively integrated over depth to obtain the overturning transport in depth:

$$\Psi_z = \int_{z_0}^{z_i} \overline{v(z)}^x \cdot L(z) \, dz \tag{2.5}$$

$\overline{(})^x$ and $\overline{(})^z$ denote zonal and vertical averages. The overturning is taken in x-direction between 2000-m isobaths and in depth above the 27.8 $kg\,m^{-3}$ isopycnal, resulting in a non-constant L. Although this isopycnal falls below 2000m depth in the central Labrador Sea, the maximum depth of the Argo profiles, this unobserved region likely contributes little to the overturning compared to higher levels and the boundary currents (Holte and Straneo, 2017; Pickart and Spall, 2007). The deviation velocity of eq. 2.4, is decomposed according to:

$$v\prime(x,z) = \overline{v\prime(x)}^z + \tilde{v}(x,z), \tag{2.6}$$

where $\tilde{v}$, the residual, denotes the baroclinic velocity field and $\overline{v\prime(x)}^z$ is the horizontal field. I then attain the horizontal overturning by multiplying the horizontal field by the depth, D, and cumulatively integrating over the distance:

$$\Psi_x = \int_{x_0}^{x_i} \overline{v\prime(x)}^z \cdot D(x)\, dx \tag{2.7}$$

In density space, I then derive the overturning by taking the sum of all transports, $v_i\, A_i$, of each grid cell over discrete density bins, ρ_j, according to:

$$\Psi(\rho_j) = \sum_{i \in \rho_j} (v_i\, A_i) \tag{2.8}$$

The overturning is then mapped back into depth space using the average depth-to-density relationship of the composite section.

While the overturning in depth space is attributed to the Eulerian sinking of water, the resolution of overturning in density space allows us to quantify the contribution of LSW formation separately. The distinction between sinking and pure water mass formation is crucial because it highlights that the volume of water transformed at the surface does not necessarily equate to the amount of water that sinks and contributes to the overturning circulation. Indeed, active convection is primarily associated with a diapycnal mass flux but not with a vertical mass flux. Sinking or downwelling within the plumes formed during convection (Marshall and Schott, 1999) is balanced by upwelling around them. Nonetheless, sinking is an essential feature in the boundary current. With a simple two-layer model of a convective basin, Straneo (2006b) showed that the boundary current becomes denser as it flows around the basin to balance the interior buoyancy loss. This density exchange is mainly induced by eddies. However, geostrophy requires that the densification of the boundary current occurs alongside sinking, thus contributing to the overturning circulation.

Despite numerous efforts, overturning and LSW formation in the Labrador Sea still need to be better constrained. Modeling and observational studies have proposed a wide range of overturning values from 1 to 7 Sv, and LSW formation estimates vary between 2 and 10 Sv (Böning et al., 1996; Delworth et al., 1993; Holte and Straneo, 2017; Pickart and Spall, 2007; Rhein et al., 2002; Talley et al., 2003; Yashayaev and Loder, 2016). Studies using different methods and data, such as large-scale velocity datasets, volume analysis, and chlorofluorocarbon inventories, have produced inconsistent results. Estimates also differ across periods with varying levels of convection, leading to a lack of consensus on the strength and variability. Potential seasonal and interannual biases further complicate this inconsistency.

Holte and Straneo (2017) examined the seasonality of overturning using an Argo float-based estimate. They derived composite sections and calculated the overturning as described above. They defined three seasons following the convective cycle. The convection season, winter, usually starts in December and ends in March. Mixed layer depths deepen throughout winter, typically reaching maximum depth and density in March. Spring then ranges from April to June, corresponding to restratification of the winter mixed layers and proposed maximum overturning. Mixed layers remain constantly shallow during the rest of the year, defined as the summer season.

Holte and Straneo (2017) found the largest overturning in spring with 1.2 Sv in depth space and 3.9 Sv in density space, attributed to the export of recently formed LSW. Overturning decreases through summer and is lowest in winter. Since Argo floats provide broad data coverage, I employed the method of Holte and Straneo, as described in the next section, to derive decadal estimates and composites based on convection intensity using the same seasons.

<div style="text-align: right; font-size: 3em;">3</div>

Data and Methods

3.1. Data

I primarily utilize depth profiles and trajectories from Argo floats collected in the Labrador Sea over the years 2002-2023 to estimate overturning. Argo is a global observing system employing a network of autonomous instruments gathering ocean data all over the globe (SEANOE, 2024). The profile data was fetched from https://erddap.ifremer.fr/erddap (ERDDAP, 2024). Following the approach of Holte and Straneo (2017), I choose the area within 75km of the AR7W line, a repeated hydrographic section crossing the Labrador Basin from Misery Point on Labrador to Cape Desolation on Greenland. The boundary outlined includes most of the deep mixed layers within the Labrador Sea, as shown in fig. 3.1, implying that a composite section from the selected profiles should effectively capture the processes of overturning and the formation of LSW. The number of profiles within the period are displayed in fig. 3.2. The total number of floats within the area is 3229 for the whole period considered.
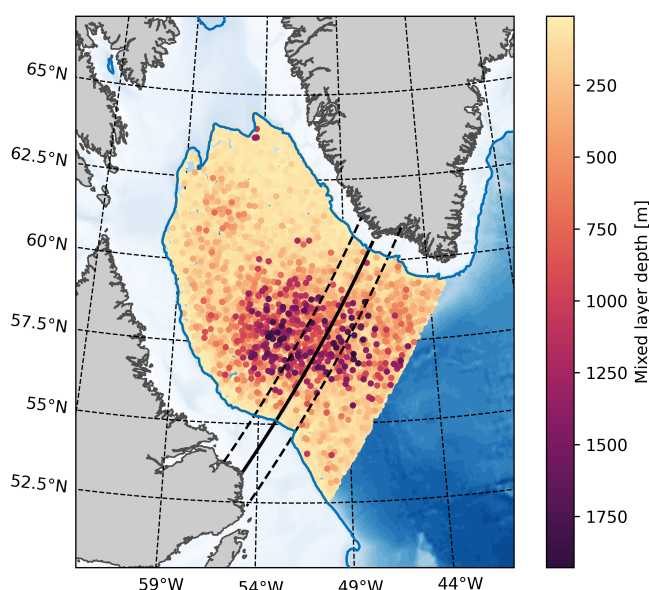
Figure 3.1: Location of Argo profiles (dots) within the period 2002-2023 and corresponding mixed layer depths (color shading) in the Labrador Sea within 1000m-isobaths (blue line). The depths are shaded in blue. The AR7W line is outlined in black, and dotted black lines denote distances of 75 km from the AR7W line.

Argo floats drift along with ocean currents, navigating between the surface and a mid-water level. The floats typically drift at a parking depth for ten days, then descend to their maximum profile pressure before ascending to the surface, measuring salinity and temperature profiles on their way up. The parking depth is typically set at 1000 *decibar* pressure, while most floats measure up to 2000 *m* depth. The vertical resolution of the profiles used mainly ranges from 1 to 10 *m*, although some parts have a coarser resolution.

For the reference velocity, I utilize the YoMaHa dataset (Lebedev et al., 2007), available at http://apdrc.soest.hawaii.edu/projects/Argo/data/trjctry/. The dataset provides velocity
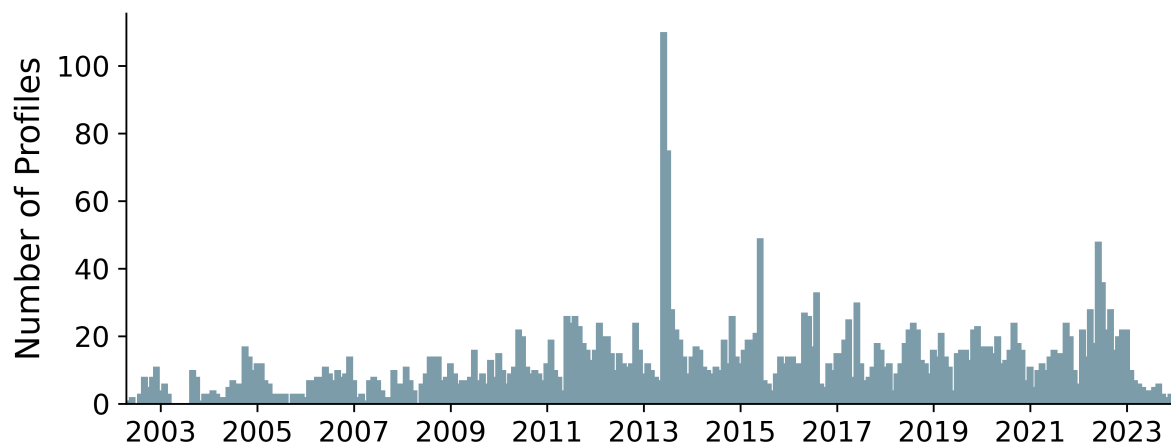
Figure 3.2: Number of profiles per month within 75 km distance from the AR7W line between 2002-2023.

data assessed from the Argo float trajectories at the parking level. The velocities are estimated from the displacement of floats during each submerged phase of the floats cycle. The errors are typically an order of magnitude smaller than the derived velocity values. The dataset provides velocity data spanning from November 2005 to May 2022 in the study region.

Additionally, I use hydrographic data from 14 surveys of the AR7W line occupied between 2002 and 2015 (see appendix for details). The data was downloaded from the CCHDO (CLIVAR and Carbon Hydrographic Data Office) website (https://cchdo.ucsd.edu/).

Conservative Temperature Θ, absolute salinity S_A and potential density σ, as well as the relative geostrophic velocity, v_{rel}, I obtain with the help of the Gibbs SeaWater (GSW) Oceanographic Toolbox of the Thermodynamic Equation Of Seawater - 2010 (TEOS-10, IOC and IAPSO, 2010).

3.2. Methods

3.2.1. Composite sections

I utilize optimal interpolation (OI) to merge the Argo profiles within 75 km of the AR7W line into composite temperature and salinity sections. OI is designed to fit irregularly spaced and sparse data (see section 3.2.2). Since the Argo floats are distributed non-uniformly across the section, mainly accumulated in the center and sparser at the shelves, OI is well-suited for accurately representing the data. The section is gridded with a 10 km horizontal resolution and 5 m vertically up to 2000 m depth. Additionally, I use the interpolation scheme to project station data from AR7W hydrographic cruises onto the same grid. From the resulting salinity and temperature sections, I compute a thermal wind field, which provides an independent shear estimate. The shear estimate is used to adjust the Argo velocities to a uniform pressure level of 1000 decibar. Following eq. 2.2 and 2.3, I utilize the Argo velocities as a reference to derive the absolute geostrophic velocity. The relative geostrophic velocity is obtained from the Argo composite sections. Finally, the overturning is derived from the absolute geostrophic velocity sections (see chapter 2).

I construct several composites using different periods. In the first step, I derive seasonal

composites for the whole period, starting in 2004 and ending in 2023. Secondly, I split the dataset into decades, selecting the periods over 2004-2013 and 2014-2023 to observe decadal changes in seasonal overturning. In both decades, years with strong deep convection and periods of weak convective activity have been observed (Yashayaev, 2024; Yashayaev and Loder, 2016, 2017). The early decade corresponds to relatively weak convection years with only a few intense convection events. The later decade includes consecutive strong convection years from 2014-2018, but also some years with shallow convection and the formation of lighter LSW. To further assess interannual changes, explicitly the impact of strong deep convection on the overturning, I lastly combine years of low and high convection intensity into composites. For the distinction between weak and strong convection years, see section 3.2.3.

To evaluate my methodology, I compare mean and seasonal overturning to the results of Holte and Straneo (2017), using the same period, ranging from March 2002 to April 2016. In contrast to my approach, they used a Laplacian spline interpolation to grid the data, a coarser vertical resolution of 25 m, and an additional velocity dataset. Also, with 1842 float profiles I use significantly more profiles than they included (1157). This may be due to different quality restraints or updated availability of quality controlled data. However, I only used data of the highest quality available which has been checked for research purposes.

3.2.2. Optimal interpolation

Optimal interpolation is a widely used method for gridding irregularly sampled data (Bretherton et al., 1976; Gasparin et al., 2015; Lavender et al., 2005; Roemmich and Gilson, 2009; Wilkin et al., 2002). This statistical technique estimates a smoothly gridded field by fitting weighted least squares to observations and a background field. One particular advantage of this method is that it provides an estimated error field alongside the interpolated data.

For my analysis, I have implemented a two dimensional modification of a specific OI technique, which is described on the website ocefpaf.github.io (Fernandes, 2014). For a more detailed description, I refer to the work of Wilkin et al. (2002). This approach involves using the data mean as the background field and calculating the mean squared misfit between a Gaussian function and the data observed at independent coordinates. Additionally, it requires input parameters such as the decorrelation length (R) and an estimated error parameter (λ). R is used to define the correlation structure of the field, which helps determine the influence of a given observation on the interpolated values at different distances.

In my two-dimensional modification, I work with two different decorrelation length scales, one horizontal scale, R_x, and one vertical scale, R_z. While R_x is kept constant, I vary R_z with depth to limit the decorrelation length in the near-surface layers since close to the surface, the ocean is influenced by more dynamic processes introducing variability at smaller spatial scales, reducing the spatial coherence of oceanographic parameters.

Since the computational cost of the OI is immense, l split the Argo dataset into chunks before interpolating. In the horizontal, I choose 150 km chunks with an overlap of 95 % percentile of the horizontal decorrelation length R_x. In the vertical, I split the data into six chunks at 100, 250, 500, 750 and 1375 m depth with overlaps of 95 % percentiles of the vertical decorrelation lengths R_z, respectively. The overlap is necessary to smooth the transition between the chunks in the resulting sections.

Various values for R_x and R_z were tested. While the results qualitatively agree, the resulting overturning values slightly differ with different decorrelation parameters and different λ. Analysing the influence of different parameters exceeds the scope of the thesis. Nonetheless, calculations with $R_x = 150\ km$ and $R_z = [30, 50, 80, 100, 120, 120]\ km$ gave good results. To further reduce the computational costs, I only pick every other data point in the vertical space. This can be done since the resolution of the Argo profiles within the periods used is substantially better in the vertical space than in the horizontal space.

3.2.3. Composites of deep convection intensity

In order to assess the interannual variability, I create groupings of years with different intensities of deep convection. A characteristic of strong convection is a deep-reaching mixed layer depth. Since the maximum mixed layer depth and densities generally occur in March and alongside maximum overturning in the spring months (Holte and Straneo, 2017), I use the maximum mixed layer depth in spring months (MAM), as well as the mean density at the derived mixed layer depth, to divide the data into years of strong and weak convection (Fig. 3.3). I define the mixed layer depth as the depth at which the density has increased by $0.01\ kg m^{-3}$ relative to the surface density.

Convection events considered substantial have typically mixed layer depths lower than 1500 m, while weak convection only reaches down to a maximum of 1000 m depth (e.g. Yashayaev, 2024; Yashayaev and Loder, 2016). Defining these 1500 m and 1000 m as thresholds, years with notable deep mixed layers and strong convective activity are 2008 and 2014-2018. Conversely , years with weak convection are 2004, 2006, 2007, 2009-2011, 2021, and 2023. The differentiation becomes more challenging for intermediate values. The maximum mixed layer depth derived from the Argo profiles in 2005 is only 100 m below the threshold depth, and 2005 is not considered a year of strong convection according to the literature (Yashayaev and Loder, 2016). Thus, I consider it a weak year. In 2012, the deep convection did not fall below 1500 m, but a steep decline in density and mixed layer depth is evident in contrast to the previous
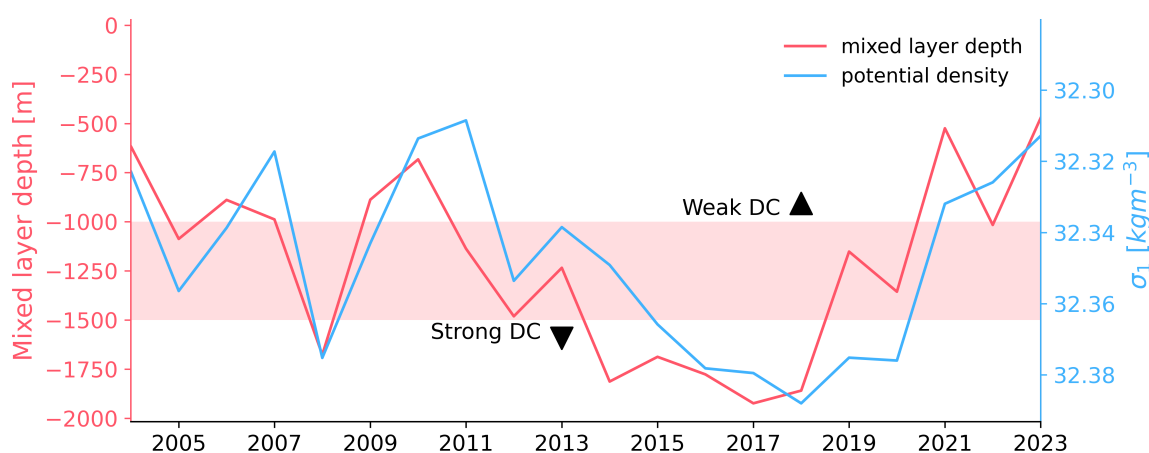
Figure 3.3: Spring mean values of maximum mixed layer depth (red) and average potential density referenced to 1000 decibar (blue) in the central Labrador Sea derived from Argo profiles within 3000m-isobaths. The red shading indicates depths of moderate deep convection (DC) in between 1000 m and 1500 m depth.

year. I therefore count 2012 as an intense event. This decline was reversed in 2013, indicating little deep convection activity despite oceanic preconditioning. Thus, I classify 2013 as a weak convection year.

The convection depths of 2019 and 2020 are relatively shallow, but the density remains as low as in previous years. In his recent paper, Yashayaev (2024) classifies both years as periods of strong convection. He reveals deeper mixed layers using a different calculative approach. The same applies for the year 2022. From my calculation, one could easily rank 2022 as a weak convection year. However, Yashayaev derived a lower depth of around 1600 m for this year. Considering that the preceding year had notably weak convection, leading to the absence of sufficient preconditioning, atmospheric forcing, particularly the North Atlantic Oscillation (NAO), had to be substantial to still induce convection (Yashayaev, 2024). Thus, 2022, 2019, and 2020 mark moderately deep convection years.

<div align="right">

4
Results

</div>

In this section, I present the main results connecting deep convection intensity and overturning. First, I show seasonal composites of the main oceanic properties for the 2004-2023 period, as well as the seasonal overturning estimates. Secondly, I show overturning estimates of the decadal composites and differences in convection intensity for all three seasons. Lastly, I provide an evaluation of the method by comparing it to the findings of Holte and Straneo(2017) for the 2002-2016 period.

4.1.   Seasonal composite sections

Fig. 4.1 shows temperature and salinity sections and the absolute geostrophic velocity across the defined seasons. The sections are derived from the Argo data within the 2004-2023 period. The absolute geostrophic velocities were referenced to the velocity fits in the upper panel of fig. 4.2. To derive a mean reference velocity, I calculated the fifth-degree polynomial fit of the running mean of the velocity data points for each season, respectively. I choose a fifth-degree fit, since this resulted in the lowest horizontal imbalances.

Seasonal hydrographic observations of the Labrador Sea are rare due to the difficulty of undertaking ship-board measurements during winter, leaving me with no direct studies for comparison. Nonetheless, the general hydrographic and velocity structures in the composite sections align with previous observations of the region (Hall et al., 2013; Holte and Straneo, 2017; Pickart and Spall, 2007; Yashayaev, 2024; Yashayaev and Loder, 2016). The interior Labrador Sea is homogeneously cold and fresh with low velocities. The seasonality is most incisive in the upper 100 m and in the boundary currents. In winter, the stratification is strong, especially at the boundaries, with cold and fresh water at the surface and relatively warm and salty water below. In the central basin, the stratification in temperature and salinity breaks, indicating vertical mixing due to convection. This area, between roughly 300 and 600 km, corresponds to the region of deepest winter mixed layers (Fig. 3.1). In spring, the upper surface layer restratifies, while the the mixing signal is still evident in the near-surface to intermediate layers. During summer, the surface warms and freshens, due to melting and freshwater export from the Arctic (Schmidt and Send, 2007).

On the eastern boundary, the West Greenland Current (WGC) advects warm saline water into the Labrador Sea. In summer, but especially in winter, notable vertical shear is observed in the boundary current. However, during spring, the current's water temperature decreases, supposedly due to colder water being advected from the Irminger Sea, resulting in a less pronounced vertical shear and fairly barotropic velocities. The water recirculates, freshens,

<div align="center">12</div>
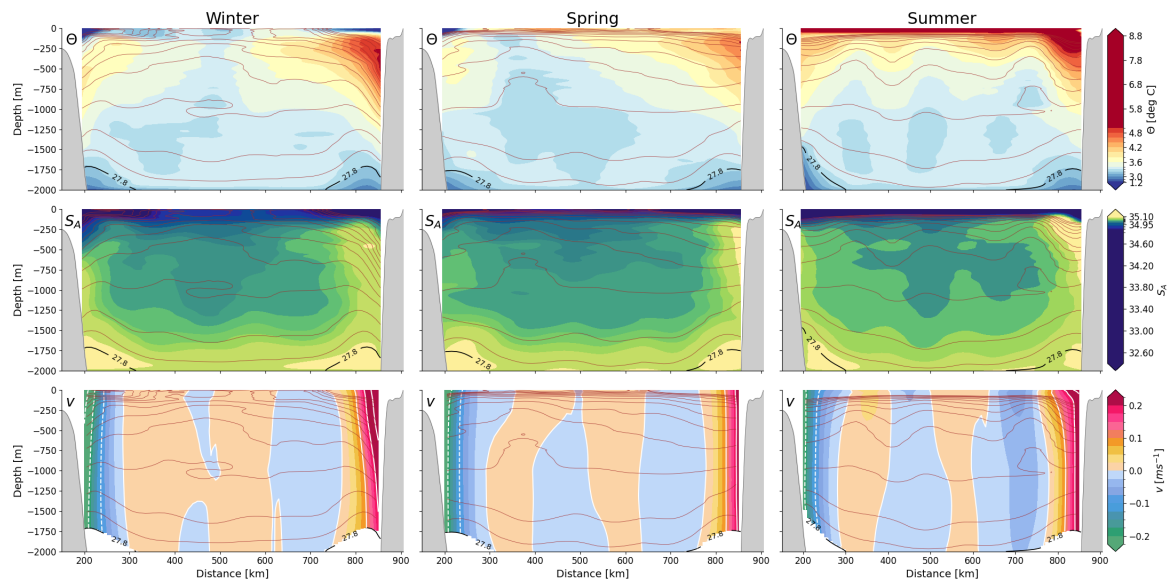
Figure 4.1: Seasonal sections across the AR7W line of conservative temperature (Θ), absolute salinity (S_A) and absolute geostrophic velocity (v) for the last two decades (2004-2023). The density (σ_0) is represented as brown contours in $0.02\ kgm^{-3}$-intervals, the $27.8\ kgm^{-3}$ contour is depicted in black.

and cools and is then advected out of the basin in the Labrador Current on the western boundary.

4.2.   Seasonal overturning

In the deepest layer of the Labrador Sea, beneath the $27.8\ kgm^{-3}$-isopycnal, the Deep Western Boundary Current (DWBC) transports overflow water from the Nordic seas throughout the basin (Dickson and Brown, 1994; Pickart and Spall, 2007). In the northern Labrador Sea, water is transported through Davis Strait. There, the water is confined to lower depths, leaving the DWBC as the only source of water transported in and out of the basin at this depth. Thus, we expect the net transport across the AR7W line in this density layer at the bottom of the sections to be zero. However, the net transports I derive from the absolute geostrophic velocities shown above increase with depths, leading to approximately 6 and 2 Sv more southward transports in spring and summer. This discrepancy might be explained by insufficient or unevenly distributed sampling coverage of the floats at the steep slopes at the eastern boundary.

Similarly to Pickart and Spall (2007), I force the transport to approach zero by adjusting the velocities at the eastern portion of the basin. Particularly, I add $c_0 = 2.5\ cm\ s^{-1}$ in spring and $c_0 = 1.0\ cm\ s^{-1}$ in summer at $x \geq 740\ km$, indicated in fig. 4.2 by the shaded gray area. This encloses the area governed by the West Greenland Current.

Contrary to the other seasons, the winter transport is slightly more northward at 2000 m depth. Nonetheless, I also force the transport to approach zero with an adjustment of $-0.2\ cms^{-1}$ at the eastern boundary to preserve consistency.

In accordance to Pickart and Spall 's results, the adjustment leads to less imbalance in the
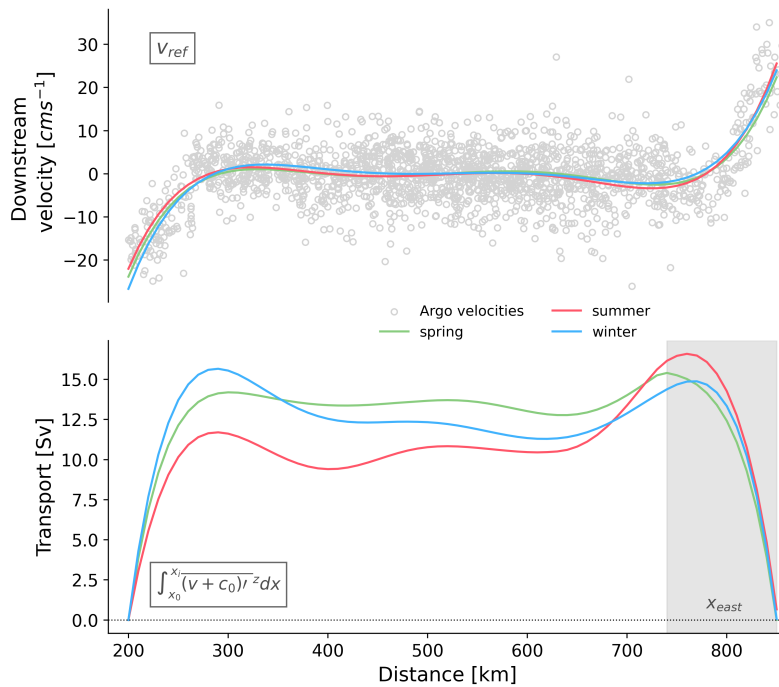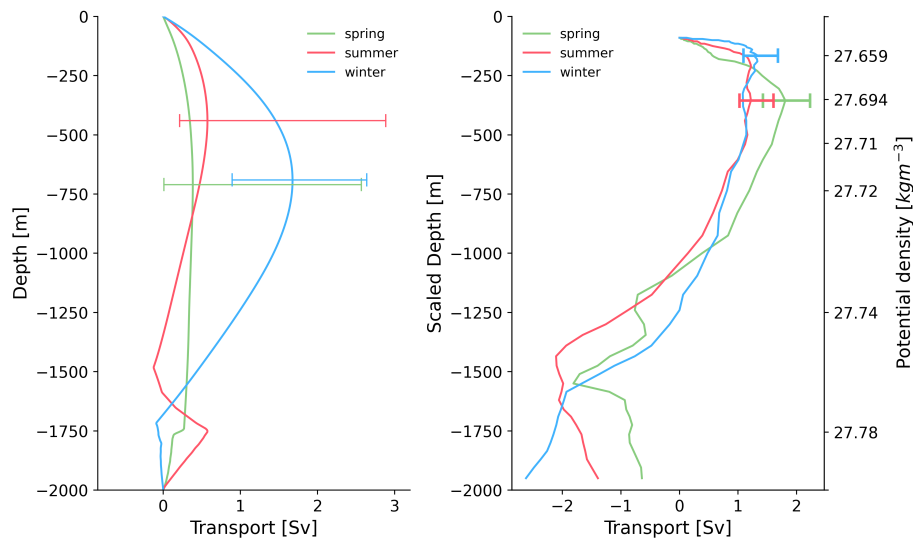
Figure 4.2: Downstream velocity adjusted to 1000 decibar (gray circles) normal to the AR7W line from Argo float trajectories between 2004-2023 (upper plot). The fits to the velocities, taken as the reference velocity, are plotted for each season (colored lines). The lower plot shows seasonal horizontal transports across the composite section above the 27.8 $kg\,m^{-3}$ isopycnal and between the 2000-m isobaths. The velocities to derive the transports are adjusted at the eastern boundary by a constant c_0.

horizontal transports in spring and in winter, for the 2004-2023 period, with only 0.01 Sv and 0.05 Sv, respectively. In contrast, the imbalance in summer is and remains higher with 0.66 Sv. The largest maximum horizontal transports in the boundary currents occur in winter in the Labrador Current (15.7 Sv) and in summer in the WGC (16.9 Sv), again for the 2004-2023 period, as depicted in the lower panel of fig. 4.2. The spring transport peaks with 15.4 Sv in the WGC and is slightly lower in the western boundary with 14.2 Sv, where the summer overturning is explicitly low with 11.7 Sv. These findings differ from the results of Holte and Straneo, who found, in general, higher transport rates and their maximum transport in both currents occurred in spring.

Above the horizontal overturning, the corresponding reference velocities are plotted. Although the seasonal differences are minimal, the sensitivity to the horizontal overturning is high (see section 4.4), therefore, most seasonal variations can be attributed to changes in the reference velocity. For example, the low transports in summer at the western boundary comply with low reference velocities.

The overturning in density and depth space are displayed in fig. 4.3. The overturning is quantified by the maximum values, MOC_z and MOC_σ in depth and density space, respectively and corresponding depths. The absolute errors indicate MOC_z and MOC_σ calculated by letting c_0 vary within $\pm 1\ cms^{-1}$. This value corresponds to estimations of the total error of absolute geostrophic velocities calculations. The error in calculating the relative velocities is quite small ($O\ 10^{-4}\ ms^{-1}$), given the high accuracy of the temperature and salinity sensors (0.002 $deg\ C$ and 0.01) and low mean estimated errors from the optimal interpolation (0.002 $deg\ C$ and 0.02). Thus, the error is dominated by the accuracy of the reference velocity, which is thought to be one magnitude smaller than the estimated velocities. Therefore, we have estimated errors in the highest velocities in the order of 1 cms^{-1}.

Figure 4.3: Seasonal overturning in depth (left) and density (right) space for the 2004-2023 periof derived from velocities adjusted by a constant c_0 at the eastern boundary. The error bars indicate MOC_z and MOC_σ respectively, calculated by letting c_0 vary within $\pm 1\ cms^{-1}$. Note that these maximum values are not necessarily at the same depths as the error bars seem to indicate.

In depth space, the maximum overturning, MOC_z, is most prominent in winter with $1.7\ Sv$ at $690\ m$ depth. In spring, the overturning shrinks to $0.4\ Sv$ but is still centered at a similar depth. In summer, the overturning shoals to a $440\ m$ depth and remains relatively small with $0.6\ Sv$. Approximated errors exceed the seasonal differences in maximum values, indicating high sensitivity to the velocity adjustment. Nonetheless, these outcomes stay in contrast to the ones of Holte and Straneo, who observed maximum overturning in spring and at lower depths for a shorter period. However, in density space, overturning is highest in spring in both cases, for the 2004-2023 period, and in Holte and Straneo's results. The spring MOC_σ adds up to $1.8\ Sv$ centered at $27.694\ kgm^{-3}$. In summer, the overturning is smaller ($1.2\ Sv$) but centered at the same density. The winter overturning is also smaller but centered at a lighter density ($1.3\ Sv$ and $27.659\ kgm^{-3}$). While the maximum overturning is less sensitive to the velocity adjustment in density space than in depth space, the overturning at $27.8\ kgm^{-3}$ increases to more southward values. Thus, the balance in depth space forced by the velocity adjustment does not translate to the overturning in density space.

4.3. Decadal variability and impacts of convection intensity

Since deep convection varies strongly on interannual to decadal time scales, influenced by variable atmospheric forcing and preconditioning of the ocean, the overturning should reflect some of these variations. Even though we experienced a decade with relatively weak convection activity between 2004-2013, followed by a decade with a consecutive period of strong deep convection, distinguishing between weak and strong convection years is necessary. This separation is crucial for drawing robust conclusions regarding the impact of deep convection and the formation of LSW).
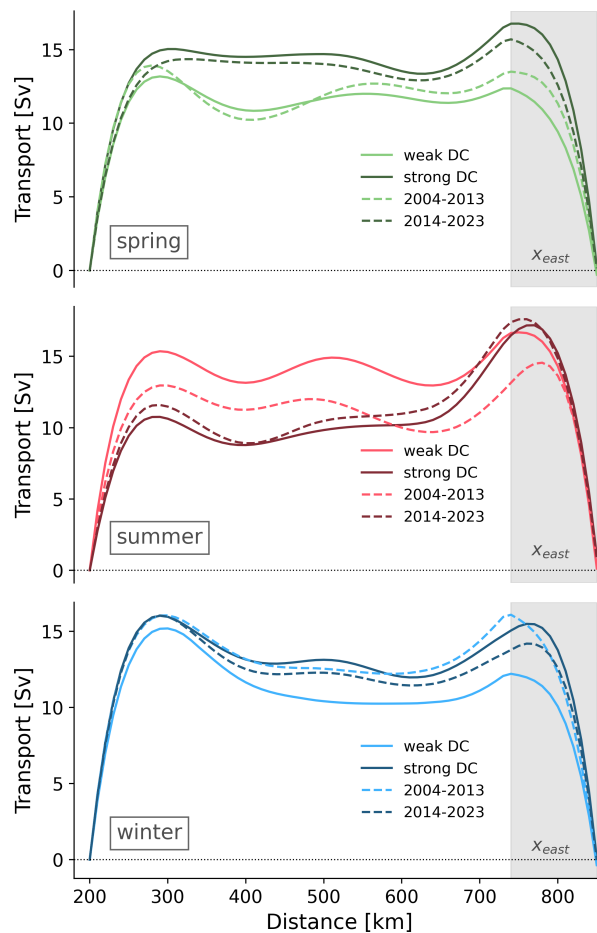
Figure 4.4: Seasonal horizontal overturning as in fig. 4.2 for strong and weak deep convection (DC) composites and both decades separately.

The distinction in strong and weak convection activity reveals generally higher horizontal transports in years of strong convection and during the later decade across the whole section in spring with maximal transports up to 16.8 Sv in the WGC at the eastern boundary (Fig. 4.4). In summer, the transports increase further in the WGC, while in the Labrador Current, the maxima decline to values smaller than the weak convection composite and the preceding decade, respectively. The Labrador Currents export increases again during winter, exceeding most spring values. In the WGC, winter transports are lower than in spring, except during the early decade (2004-2013), when atypical high values occur.

In accordance with the mean seasonal overturning, the overturning in depth space is highest in winter, reaching 1.7, 1.5, and 1.6 Sv for the composites of strong convection years, weak convection years, and the decade between 2014-2023, respectively (Fig. 4.5). In the early decade, however, we have exceptionally low values throughout the water column, and the maximum MOC_z occurs at 1505 m depth. This occurrence, which is also evident in the 2014-2023 summer period, might be an artifact of the adjustment made or the exclusion of velocities below 27.8 $kg\,m^{-3}$ in the overturning calculations, which leads to inflections at corresponding depths. Still, the low transport in the early decade agrees with Holte and Straneo's results . In contrast, the weak convection composite shows similar transports to the strong convection composite, albeit slightly lower and centered at a shallower depth . Accordingly, the low winter transports can not be attributed to low convection intensity with certainty.

In summer, the strong convection composite shows again the highest transports. The weak convection composite has exceptionally low transports, indicating a plausible link to convection intensity that persists during summer restratification. Notably, the later decade shows lower transports than the 2004-2013 period, suggesting different mechanisms leading to decadal variations, albeit not robust.

The differences in strong and weak convection composites, as well as the decadal variations, are also prominent in spring, with higher MOC_z at lower depths for the strong convection

composite and the later decade. Thus, although the transports are lower than winter values, a link to deep convection intensity is evident.

The link between intense convection and overturning in the Labrador Sea persists in density space (Fig. 4.6). Here, we observe the highest overturning values centered at the greatest densities in spring during strong convection years (3.4 Sv) and the 2014-2023 period (2.7 Sv). Both maxima occur at a density of 27.73 kgm^{-1}, which corresponds to intermediate values of what is usually defined as LSW (Kostov et al., 2024). In winter and summer, the MOC_σ is weaker and centered around lighter densities. However, high imbalances in depth space, as observed in the mean seasonal overturning, and high horizontal imbalances, primarily in summer, are evident. Despite this, the winter and summer MOC_σ show minor sensitivity due to the velocity adjustment, implying some robustness.
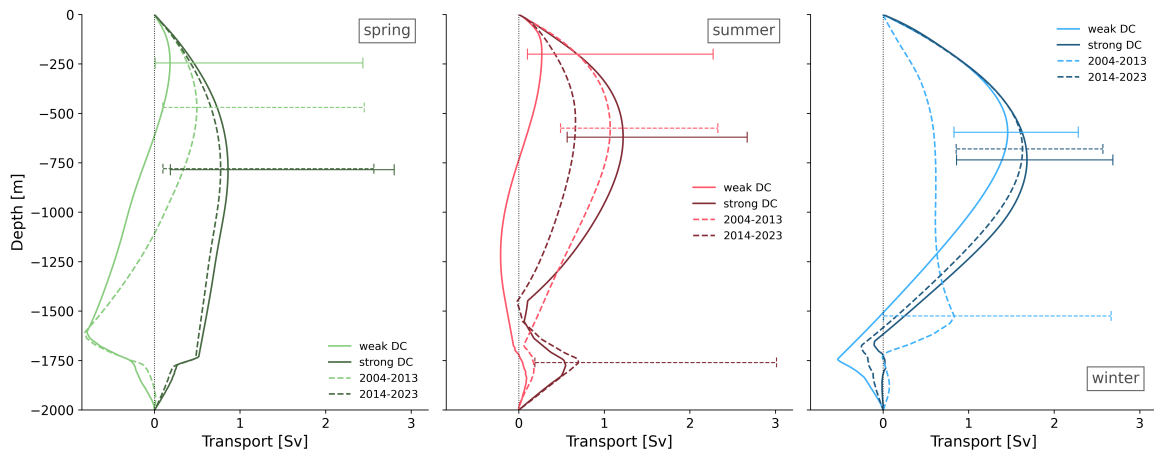
Figure 4.5: Seasonal overturning in depth space as in fig. 4.3 for strong and weak deep convection (DC) composites (solid lines) and both decades separately (dashed lines).
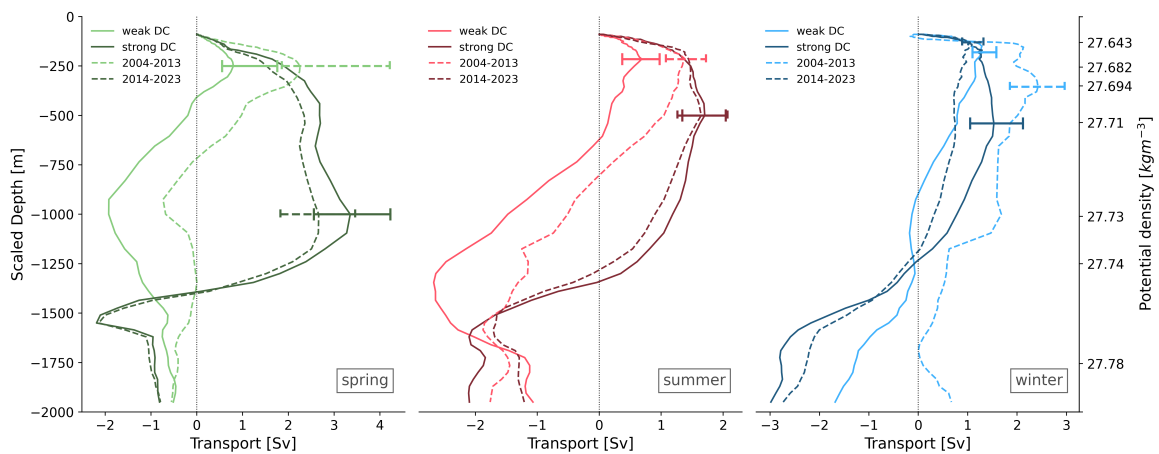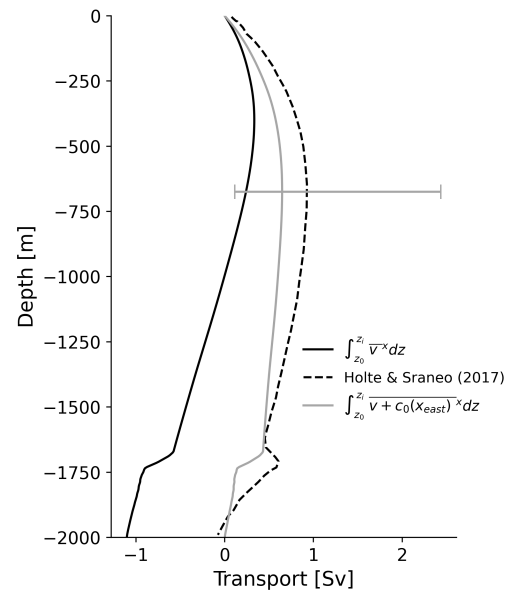

Figure 4.6: Same as in fig. 4.5 but in density space.

## 4.4.   Evaluation of the methodology

To be able to assess the suitability of my method, especially regarding the velocity adjustment made and the reference velocity, I test the sensitivity induced by both and compare my results to the estimates of Holte and Straneo (2017).

Sensitivity to the velocity adjustment   In contrast to Holte and Straneo's (2017) findings, the mean overturning in depth space I obtain for the period from March 2002 to April 2016 is not balanced (black curve, Fig. 4.7). As discussed before, I therefore adjust the velocities by $c_0 = 0.50 \, cm \, s^{-1}$ at $x \geq 740 \, km$ to approach zero at the bottom of my section. The overturning derived from the adjusted velocities aligns closely to the overturning of Holte and Straneo, the MOC_z is 0.65 Sv and occurs at 675 m depth, which is smaller than the estimate of Holte and Straneo, and occurs at the same depth. While the densities where maximum overturning occurs are identical, the maximum transport in density space and the horizontal transports are weaker in my estimate, particularly in the WGC (see appendix). Albeit Holte and Straneo's mean estimate is not necessarily more correct than


Figure 4.7: Mean vertical transport between March 2002 and April 2016 (black), mean transport extracted from Holte and Straneo(2017) (dashed), and adjusted mean vertical transport (gray).

mine, they utilized Monte-Carlo experiments to test the robustness of their findings. The mean overturning I derive lies inside their estimated standard deviations, suggesting confidence in my approach to adjust the eastern velocities. To test the sensitivity induced by adjusting the velocities, I calculate ΔMOC, Δz_{MOC} in depth and density space and the change in the horizontal imbalance as a function of $c_0 \pm 2 \, cms^{-1}$ (Fig. 4.8). Decreasing c_0 by 1 cms^{-1}, leads to changes in MOC_z and MOC_σ of −0.53 and −0.39 Sv. Increasing c_0 by 1 cms^{-1} leads to an increase of 1.79 Sv in MOC_z due to a shift to significantly lower z_{MOC_z}. In density space, z_{MOC_σ} remains fairly constant and shifts to higher values close before the 2 cms^{-1}-increase in c_0. The horizontal imbalance changes linearly with a change in c_0, albeit the changes are small with maximal 0.1 Sv.

Sensitivity to the reference velocity   The portion of the overturning induced by the reference velocity for the 2002-2016 period is exceptionally high in the horizontal overturning, reflected by small to no differences in the boundary currents and differences of maximal 1.4 Sv in the center of the section (fig. 4.9). The high sensitivity at the boundaries is attributed to the high absolute values of the reference velocities in the boundaries compared to small relative velocities throughout the section, emphasizing the need for accurate reference data.

In depth space, the reference velocity is averaged over the section, adding a constant to the velocity, leading to a linear decrease in the cumulative integration up to the depth where the density in the boundaries reaches 27.8 kgm^{-3} and the reference velocities are averaged over a
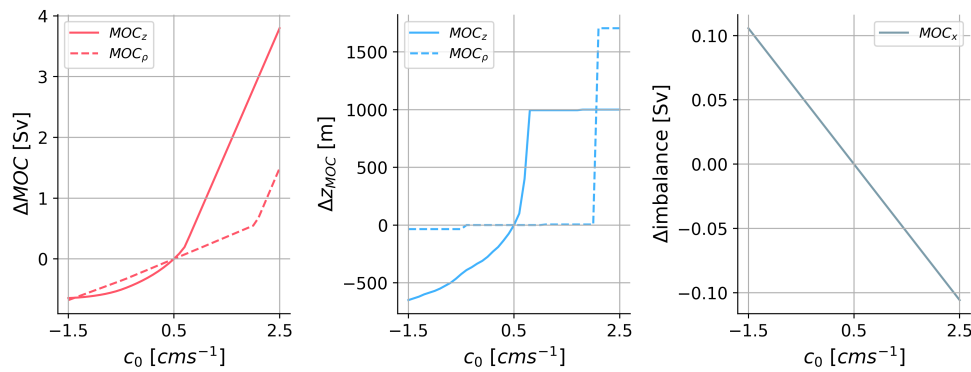
Figure 4.8: Induced changes by the adjustment of the reference velocity in the maximum overturning in depth and density space (MOC) (left), the depth of maximum transport, z_{MOC} (center), and the imbalance across the section (right), all as a function of the constant added to the eastern portion, $c_0 \pm 2\ cms^{-1}$ for the 2002-2016 period.

smaller section. The impact of the reference velocity in depth space is nearly constant across the water column but still affects the maximum overturning. In this case, MOC_z is reduced. For other periods and different c_0, the effect of the reference velocity might be opposite, with a linear increase in depth leading to an augmentation of MOC_z.

Additionally, I tested several fits of the reference velocity, using higher-degree polynomials and including more data points at the boundaries outside the actual section to derive the fit (see appendix). In general, the vertical imbalance highly differs using different fits. On the other hand, the velocity adjustment compensates for those imbalances. In the horizontal, the main differences lie in the boundaries resulting in slightly different overturning maxima, again emphasizing the need for careful measurements of the reference velocity.
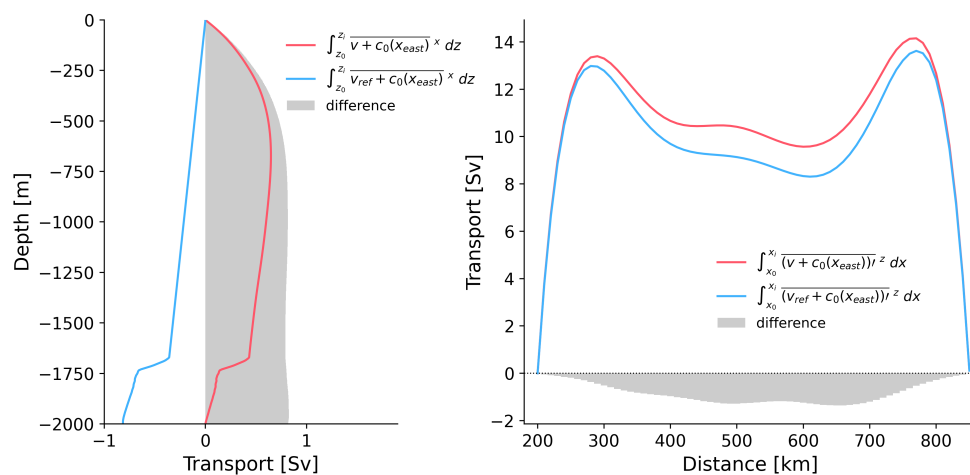
Figure 4.9: Overturning in depth (left panel, red line) compared to the overturning induced by the reference velocity (left panel, blue line) and their difference (gray shading) for the 2002-2016 period, both adjusted with equivalent c_0. Same for mean horizontal overturning (right panel).

5
Discussion

The results presented provide further insight into our understanding and quantification of the overturning circulation's strength and variability while at the same time underlining the need for carefully constructed estimates.

The seasonal overturning composites I obtain for 2004-2023 differ from the findings of Holte and Straneo (2017), who investigated a smaller period between 2002-2016. In general, the transports I calculate are lower. Nonetheless, my results support the idea of intensified spring overturning due to the export of LSW. I also find the highest overturning in density space occurring in spring. The overturning is centered at 27.694 $kg m^{-3}$, a slightly greater density than the one derived by Holte and Straneo, which is reasonable, considering the period I use encloses the recent intensification of convection. The decomposition by decades and convection intensity further underscores the strong connection between LSW formation and spring overturning. It reveals significantly higher transports centered at greater densities during years of strong convection and in the recent decade.

Horizontal overturning in the Labrador Current is similarly enhanced in spring for the more extended period but is also highest in winter. Accordingly, the winter overturning in depth space, associated with sinking, exceeds the overturning in spring and summer. This suggests that winter overturning is intensified during the period which includes the recent reoccurrence of intense convection. The enhancement of winter overturning may be due to increased sinking in the boundary current triggered by the densification in the interior. In contrast to the export of LSW in spring, this feedback seems more direct since it occurs during the convective season rather than in the months after. However, the decomposition by decades and convection intensity reveals more complexity. In agreement with the evident intensification during winter, the overturning estimates in depth space in winter are highest for the strong convection composite and lowest for the early decade, aligning with Holte and Straneo's findings. Nevertheless, winter convection remains high during years of weak convection, which questions the role of convection intensity in enhancing overturning in winter and might hint to other processes at place.

The seasonal composite sections of temperature, salinity, and absolute geostrophic velocities reveal a seasonal cycle strongly dependent on deep convection, which agrees with the literature. In winter, we see vertical mixing, which can be attributed to deep convection in the central Labrador Sea. The mixed layers are still evident in spring when restratification of the surface layer sets in. An outstanding feature of the velocity section is the reduction of shear coinciding with lower temperatures in the West Greenland Current in spring. The decrease in temperature might be related to cold water imported from the Irminger Sea, which also affects the local shear. Both factors may contribute to the notably low spring overturning

associated with sinking during the 2004-2023 period. The lighter densities indicate reduced buoyancy forces inhibiting sinking in the boundary current. Similarly, lower shear suggests a more stable flow, potentially correlating with reduced sinking and vertical mixing. This underscores the important role of sinking in the boundary currents and stays in contrast to the more pronounced overturning occurring simultaneously in density space, attributed to the formation of LSW in the central basin.

Although the findings align primarily with the literature and can be explained by physical processes, it is essential to emphasize the limitations of the method.

A velocity adjustment at the eastern part of the basin was necessary to balance the transport in depth space at the boundary, ensuring no net transport at $27.8\ kg m^{-3}$. While the adjustment results in less horizontal imbalance in spring and winter, the imbalance in summer remains relatively high at $0.66\ Sv$. However, this lies within the accepted imbalance of $\pm 2\ Sv$ Holte and Straneo used in the bootstrapping estimates to gauge the error in their mean overturning. The resulting standard deviation is $0.5\ Sv$ in depth space, indicating that the sensitivity to horizontal imbalances is in that order. Nevertheless, the sensitivity to the velocity adjustment is high in the mean overturning, especially in depth space as described in section 4.4. Small changes in c_0 that lie within the estimated accuracy of $1\ cm s^{-1}$ lead to differences in MOC_z in the same order as the standard deviation of Holte and Straneo for a reduction of c_0. Increasing c_0 reveals substantially higher values. Accordingly, the depth of maximum overturning jumps to unreasonably low values. In density space, the sensitivity to the adjustment is lower, but the overturning does not approach zero at $27.8\ kg m^{-3}$, questioning the justification of the velocity adjustment.

Unfortunately, I could not provide error estimates for the overturning composites apart from the sensitivity induced by the velocity adjustment. The computational costs of optimal interpolation are substantially high, making statistical approaches to gauge errors, such as bootstrap estimates, infeasible. Consequently, the results should be interpreted cautiously, as the potential error margins remain unquantified.

Even so, the estimated accuracy of the relative geostrophic velocities produced by optimal interpolation is relatively small within the order of $10^{-4}\ ms^{-1}$. In contrast, the error induced by the absolute velocities by the reference velocity fit is higher. The estimated errors of the trajectory data used to derive the reference velocity are in the order of $10^{-2}\ ms^{-1}$, and unknown sources of error induced by different choices of fitting add to that uncertainty. Therefore, the error is governed by the reference velocity fit, and it might be sufficient to estimate the total error by applying Monte-Carlo experiments only to the reference velocity and leaving the OI-derived relative velocity field constant as a next step. Nonetheless, this highlights the importance of accurate velocity data to derive overturning estimates in the Labrador Sea. One could consider using additional datasets, such as satellite-based data, to obtain more accurate reference velocities. Additionally, one could experiment with varying sampling coverage of the floats near the boundaries to test the persistence and possible origins of the high imbalances found in the vertical overturning field.

6
Conclusion

This thesis has examined the decadal variability of local overturning circulation in the Labrador Sea, with a focus on the relation between deep convection and overturning intensity. Utilizing Argo float data and optimal interpolation, I constructed seasonal and decadal composites to analyze the impact of deep convection on local overturning.

The findings of this study underscore the significant role of deep convection in driving local overturning variability in the Labrador Sea. The analysis reveals that years with strong deep convection are associated with more vigorous overturning. In particular, overturning attributed to the formation of Labrador Sea water is enhanced in spring with maximum transports of $3.4\,Sv$ centered at $27.73\,kg\,m^{-3}$, corresponding to the outlflow of previous formed LSW. In depth space, strongest overturning occurs in winter ($1.7\,Sv$), possibly associated with sinking in the boundary current. Yet, this cannot be definitively linked to convection intensity, as the weak convection composite exhibits similarly strong overturning. Moreover, the results suggest a decadal variability in winter convection, indicating that overturning strength in winter fluctuates over longer time scales due to other processes.

The methodology employed in this thesis, including the use of optimal interpolation and a velocity adjustment, proved effective in capturing the overturning circulation. However, the sensitivity analysis indicates the importance of accurate reference velocity measurements and the need for robust error estimation techniques to enhance the reliability of future studies.

Overall, this thesis contributes to a deeper understanding of the interplay between deep convection and overturning in the Labrador Sea. It underscores the critical need for long-term observational datasets to better predict the implications of climate change on the AMOC. Future research should aim to refine the methodologies used for estimating overturning and explore the potential impacts of ongoing climate change on deep convection processes.

Acknowledgement

I would like to thank my supervisors for their guidance, support, and encouragement throughout the course of my research. I am deeply grateful to my friends and family for their support and understanding during this journey. Your encouragement has been a source of strength and motivation for me. A special thank you to my office mates, whose companionship and discussions have made this experience enjoyable and enriching. Thank you all for your contributions to the completion of this thesis.

References

Böning, C. W., Behrens, E., Biastoch, A., Getzlaff, K., & Bamber, J. L. (2016). Emerging impact of greenland meltwater on deepwater formation in the north atlantic ocean. *Nature Geoscience*, *9*, 523–527. https://doi.org/10.1038/ngeo2740

Böning, C. W., Scheinert, M., Dengg, J., Biastoch, A., & Funk, A. (2006). Decadal variability of subpolar gyre transport and its reverberation in the north atlantic overturning. *Geophysical Research Letters*, *33*, L21S01. https://doi.org/10.1029/2006GL026906

Böning, C. W., Bryan, F. O., Holland, W. R., & Döscher, R. (1996). Deep-water formation and meridional overturning in a high-resolution model of the north atlantic. *Journal of Physical Oceanography*, *26*(7), 1142–1164. https://doi.org/10.1175/1520-0485(1996)026<1142:DWFAMO>2.0.CO;2

Böning, C. W., Wagner, P., Handmann, P., Schwarzkopf, F. U., Getzlaff, K., & Biastoch, A. (2023). Decadal changes in atlantic overturning due to the excessive 1990s labrador sea convection. *Nature communications*, *14*(1), 4635. https://doi.org/10.1038/s41467-023-40323-9

Bretherton, F. P., Davis, R. E., & Fandry, C. (1976). A technique for objective analysis and design of oceanographic experiments applied to mode-73. *Deep Sea Research and Oceanographic Abstracts*, *23*(7), 559–582. https://doi.org/10.1016/0011-7471(76)90001-2

Chomiak, L., Volkov, D., & Schmid, C. (2023). The interior spreading story of labrador sea water. *Frontiers in Marine Science*, *10*, 1270463. https://doi.org/10.3389/fmars.2023.1270463

Delworth, T., Manabe, S., & Stouffer, R. J. (1993). Interdecadal variations of the thermohaline circulation in a coupled ocean-atmosphere model. *Journal of Climate*, *6*(11), 1993–2011. https://doi.org/10.1175/1520-0442(1993)006<1993:IVOTTC>2.0.CO;2

Desbruyères, D. G., Mercier, H., Maze, G., & Daniault, N. (2019). Surface predictor of overturning circulation and heat content change in the subpolar north atlantic. *Ocean Science*, *15*(3), 809–817. https://doi.org/SurfacepredictorofoverturningcirculationandheatcontentchangeinthesubpolarNorthAtlantic

Dickson, R. R., & Brown, J. (1994). The production of north atlantic deep water: Sources, rates, and pathways. *Journal of Geophysical Research: Oceans*, *99*(C6), 12319–12341. https://doi.org/10.1029/94JC00530

Drijfhout, S., et al. (2015). Catalogue of abrupt shifts in intergovernmental panel on climate change climate models. *Proceedings of the National Academy of Sciences of the United States of America*, *112*, E5777–E5786. https://doi.org/10.1073/pnas.1511451112

ERDDAP, I. (2024). ARGO Dataset [Fetched date: 2024/03/25]. https://doi.org/10.17882/42182

Fanning, A. F., & Weaver, A. J. (1997). A horizontal resolution and parameter sensitivity study of heat transport in an idealized coupled climate model. *Journal of climate*, *10*(10), 2469–2478. https://doi.org/10.1175/1520-0442(1997)010%3C2469:AHRAPS%3E2.0.CO;2

Fernandes, F. (2014). Optimum interpolation [Accessed: 2024-07-01].

Gasparin, F., Roemmich, D., Gilson, J., & Cornuelle, B. (2015). Assessment of the upper-ocean observing system in the equatorial pacific: The role of argo in resolving intraseasonal to

interannual variability. *Journal of Atmospheric and Oceanic Technology*, *32*(9), 1668–1688. https://doi.org/10.1175/JTECH-D-14-00218.1

Hall, M. M., Torres, D. J., & Yashayaev, I. (2013). Absolute velocity along the ar7w section in the labrador sea. *Deep Sea Research Part I: Oceanographic Research Papers*, *72*, 72–87. https://doi.org/10.1002/2016GL071668

Holte, J., & Straneo, F. (2017). Seasonal overturning of the labrador sea as observed by argo floats. *Journal of Physical Oceanography*, *47*(10), 2531–2543. https://doi.org/10.1175/JPO-D-17-0051.1

IOC, S., & IAPSO. (2010). *The international thermodynamic equation of seawater—2010: Calculation and use of thermodynamic properties*. Intergovernmental Oceanographic Commission. http://www.teos-10.org/pubs/TEOS-10_Manual.pdf

Jackson, L. C., Peterson, K. A., Roberts, C. D., & Wood, R. A. (2016). Recent slowing of atlantic overturning circulation as a recovery from earlier strengthening. *Nature Geoscience*, *9*(7), 518–522. https://doi.org/10.1038/ngeo2715

Kostov, Y., Messias, M.-J., Mercier, H., Marshall, D. P., & Johnson, H. L. (2024). Surface factors controlling the volume of accumulated labrador sea water. *Ocean Science*, *20*(2), 521–547. https://doi.org/10.5194/os-20-521-2024

Lavender, K. L., Owens, W. B., & Davis, R. E. (2005). The mid-depth circulation of the subpolar north atlantic ocean as measured by subsurface floats. *Deep Sea Research Part I: Oceanographic Research Papers*, *52*(5), 767–785. https://doi.org/10.1016/j.dsr.2004.12.007

Lazier, J., Hendry, R., Clarke, A., Yashayaev, I., & Rhines, P. (2002). Convection and restratification in the labrador sea, 1990–2000. *Deep Sea Research Part I: Oceanographic Research Papers*, *49*(10), 1819–1835. https://doi.org/10.1016/S0967-0637(02)00064-X

Le Bras, I. A.-A. (2023). Labrador sea water spreading and the atlantic meridional overturning circulation. *Philosophical Transactions of the Royal Society A*, *381*(2262), 20220189. https://doi.org/10.1098/rsta.2022.0189

Le Bras, I. A.-A., Willis, J., & Fenty, I. (2023). The atlantic meridional overturning circulation at 35 n from deep moorings, floats, and satellite altimeter. *Geophysical Research Letters*, *50*(10), e2022GL101931. https://doi.org/10.1029/2022GL101931

Lebedev, K., Yoshinari, H., Maximenko, N., & Hacker, P. (2007). *YoMaHa'07: Velocity data assessed from trajectories of Argo floats at parking level and at the sea surface* (Tech. Note No. 4). International Pacific Research Center, University of Hawaii. http://apdrc.soest

Li, F., Lozier, M. S., Bacon, S., Bower, A., Cunningham, S., De Jong, M., DeYoung, B., Fraser, N., Fried, N., Han, G., et al. (2021). Subpolar north atlantic western boundary density anomalies and the meridional overturning circulation. *Nature Communications*, *12*(1), 3002. https://doi.org/10.1038/s41467-021-23350-2

Lozier, M. S., Li, F., Bacon, S., Bahr, F., Bower, A. S., Cunningham, S., de Jong, M. F., de Steur, L., deYoung, B., Fischer, J., et al. (2019). A sea change in our view of overturning in the subpolar north atlantic. *Science*, *363*(6426), 516–521. https://doi.org/10.1126/science.aau6592

Marshall, J., & Schott, F. (1999). Open-ocean convection: Observations, theory, and models. *Reviews of geophysics*, *37*(1), 1–64. https://doi.org/10.1029/98RG02739

Pickart, R. S., & Spall, M. A. (2007). Impact of labrador sea convection on the north atlantic meridional overturning circulation. *Journal of Physical Oceanography*, *37*(9), 2207–2227. https://doi.org/10.1175/JPO3178.1

Pickart, R. S., Torres, D. J., & Clarke, R. A. (2002). Hydrography of the labrador sea during active convection. *Journal of Physical Oceanography*, *32*(2), 428–457. https://doi.org/10.1175/1520-0485(2002)032<0428:HOTLSD>2.0.CO;2

Rhein, M., Fischer, J., Smethie, W. M., Smythe-Wright, D., Weiss, R. F., Mertens, C., Min, D.-H., Fleischmann, U., & Putzka, A. (2002). Labrador sea water: Pathways, cfc inventory, and formation rates. *Journal of Physical Oceanography*, *32*(2), 648–665. https://doi.org/10.1175/1520-0485(2002)032%3C0648:LSWPCI%3E2.0.CO;2

Roemmich, D., & Gilson, J. (2009). The 2004–2008 mean and annual cycle of temperature, salinity, and steric height in the global ocean from the argo program. *Progress in oceanography*, *82*(2), 81–100. https://doi.org/10.1016/j.pocean.2009.03.004

Schmidt, S., & Send, U. (2007). Origin and composition of seasonal labrador sea freshwater. *Journal of Physical Oceanography*, *37*(6), 1445–1454. https://doi.org/10.1175/JPO3065.1

SEANOE. (2024). Data repository of SEANOE [Accessed: 2024-06-29]. https://doi.org/10.17882/42182

Straneo, F. (2006a). Heat and freshwater transport through the central labrador sea. *Journal of Physical Oceanography*, *36*(4), 606–628. https://doi.org/10.1175/JPO2875.1

Straneo, F. (2006b). On the connection between dense water formation, overturning, and poleward heat transport in a convective basin. *Journal of Physical Oceanography*, *36*(9), 1822–1840. https://doi.org/10.1175/JPO2932.1

Straneo, F., Pickart, R. S., & Lavender, K. (2003). Spreading of labrador sea water: An advective-diffusive study based on lagrangian data. *Deep Sea Research Part I: Oceanographic Research Papers*, *50*(6), 701–719. https://doi.org/10.1016/S0967-0637(03)00057-8

Talley, L. D., & McCartney, M. S. (1982). Distribution and circulation of labrador sea water. *Journal of Physical Oceanography*, *12*(11), 1189–1205. https://doi.org/10.1175/1520-0485(1982)012<1189:DACOLS>2.0.CO;2

Talley, L. D., Reid, J. L., & Robbins, P. E. (2003). Data-based meridional overturning streamfunctions for the global ocean. *Journal of Climate*, *16*(19), 3213–3226. https://doi.org/10.1175/1520-0442(2003)016<3213:DMOSFT>2.0.CO;2

Våge, K., Pickart, R. S., Thierry, V., Reverdin, G., Lee, C. M., Petrie, B., Agnew, T. A., Wong, A., & Ribergaard, M. H. (2009). Surprising return of deep convection to the subpolar north atlantic ocean in winter 2007–2008. *Nature Geoscience*, *2*(1), 67–72. https://doi.org/10.1038/ngeo382

van Sebille, E., Baringer, M. O., Johns, W. E., Meinen, C. S., Beal, L. M., de Jong, M. F., & van Aken, H. M. (2011). Propagation pathways of classical labrador sea water from its source region to 26°n. *Journal of Geophysical Research: Oceans*, *116*(C12). https://doi.org/10.1029/2011JC007171

Wilkin, J. L., Bowen, M. M., & Emery, W. J. (2002). Mapping mesoscale currents by optimal interpolation of satellite radiometer and altimeter data. *Ocean Dynamics*, *52*, 95–103. https://doi.org/10.1007/s10236-001-0011-2

Yashayaev, I. (2024). Intensification and shutdown of deep convection in the labrador sea were caused by changes in atmospheric and freshwater dynamics. *Communications Earth & Environment*, *5*(1), 156. https://doi.org/10.1038/s43247-024-01296-9

Yashayaev, I., Bersch, M., & van Aken, H. M. (2007). Spreading of the labrador sea water to the irminger and iceland basins. *Geophysical Research Letters*, *34*(10). https://doi.org/10.1175/1520-0485(2002)032%3C0648:LSWPCI%3E2.0.CO;2

Yashayaev, I., & Loder, J. W. (2016). Recurrent replenishment of l abrador s ea w ater and associated decadal-scale variability. *Journal of Geophysical Research: Oceans*, *121*(11), 8095–8114. https://doi.org/10.1002/2016JC012046

Yashayaev, I., & Loder, J. W. (2017). Further intensification of deep convection in the labrador sea in 2016. *Geophysical Research Letters*, *44*(3), 1429–1438.

Yeager, S. G., & Danabasoglu, G. (2012). Sensitivity of atlantic meridional overturning circulation variability to parameterized nordic sea overflows in ccsm4. *Journal of Climate*, *25*, 2077–2103. https://doi.org/10.1175/JCLI-D-11-00149.1

Yeager, S., Castruccio, F., Chang, P., Danabasoglu, G., Maroon, E., Small, J., Wang, H., Wu, L., & Zhang, S. (2021). An outsized role for the labrador sea in the multidecadal variability of the atlantic overturning circulation. *Science Advances*, *7*(41), eabh3592. https://doi.org/10.1126/sciadv.abh3592

Zou, S., & Lozier, M. S. (2016). Breaking the linkage between labrador sea water production and its advective export to the subtropical gyre. *Journal of Physical Oceanography*, *46*(7), 2169–2182. https://doi.org/10.1175/JPO-D-15-0210.1
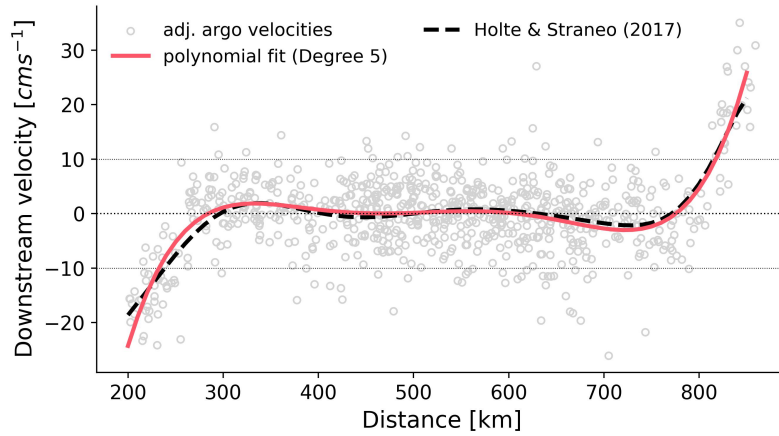
Figure 1: Downstream velocity adjusted to 1000 decibar (gray circles) normal to the AR7W line from Argo float trajectories between May 2002 - April 2016. The fit to the velocities, taken as the reference velocity, is plotted in red, alongside the reference velocity extracted from Holte and Straneo (2017) (dashed line). plotted.
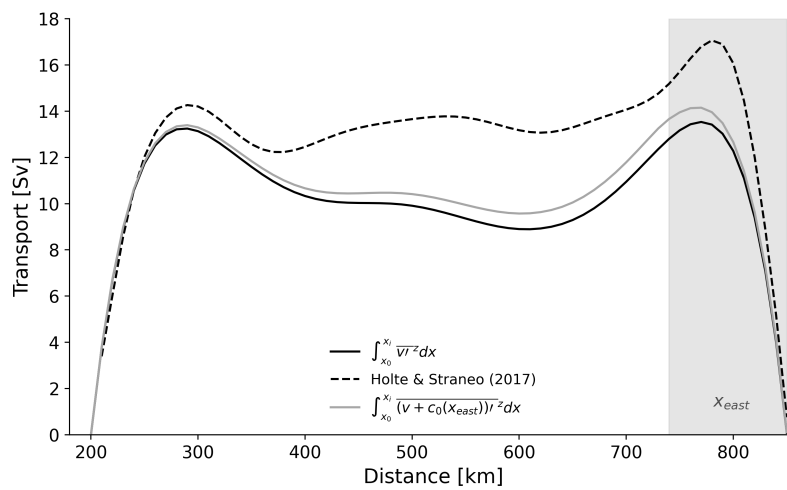
Figure 2: Mean horizontal transport between March 2002 and April 2016 (black), mean transport extracted from Holte and Straneo (2017) (dashed), and adjusted mean horizontal transport (gray).
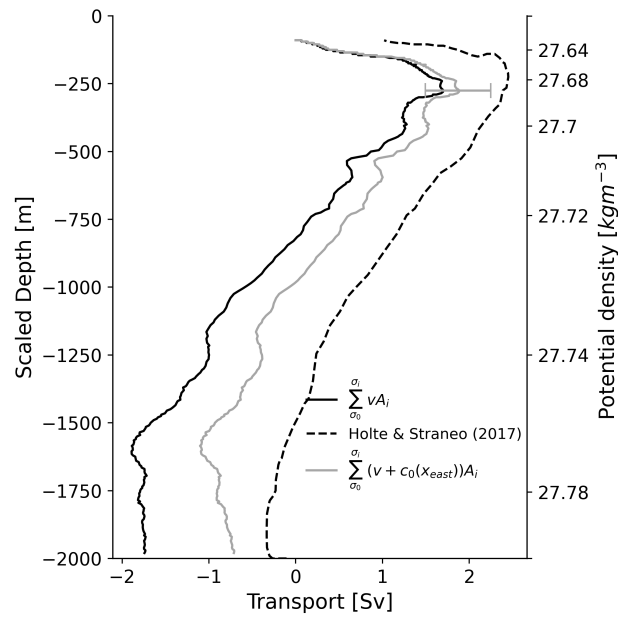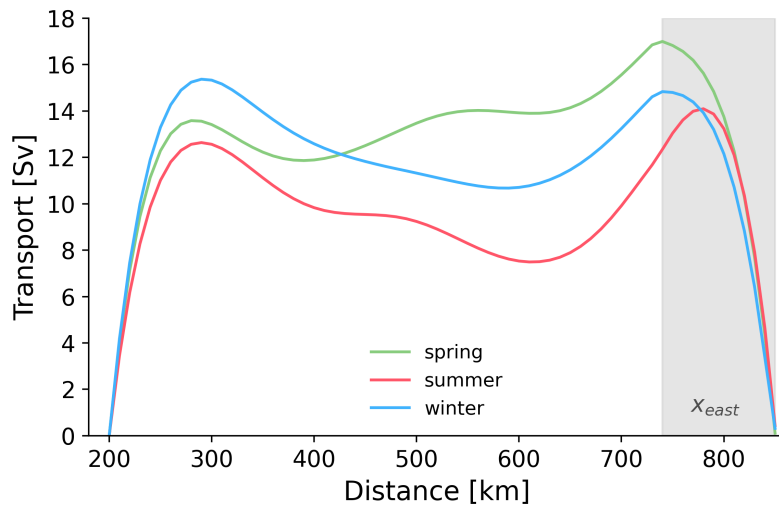
Figure 3: Overturning in depth space between March 2002 and April 2016 (black), mean transport extracted from Holte and Straneo (2017) (dashed), and adjusted overturning (gray)
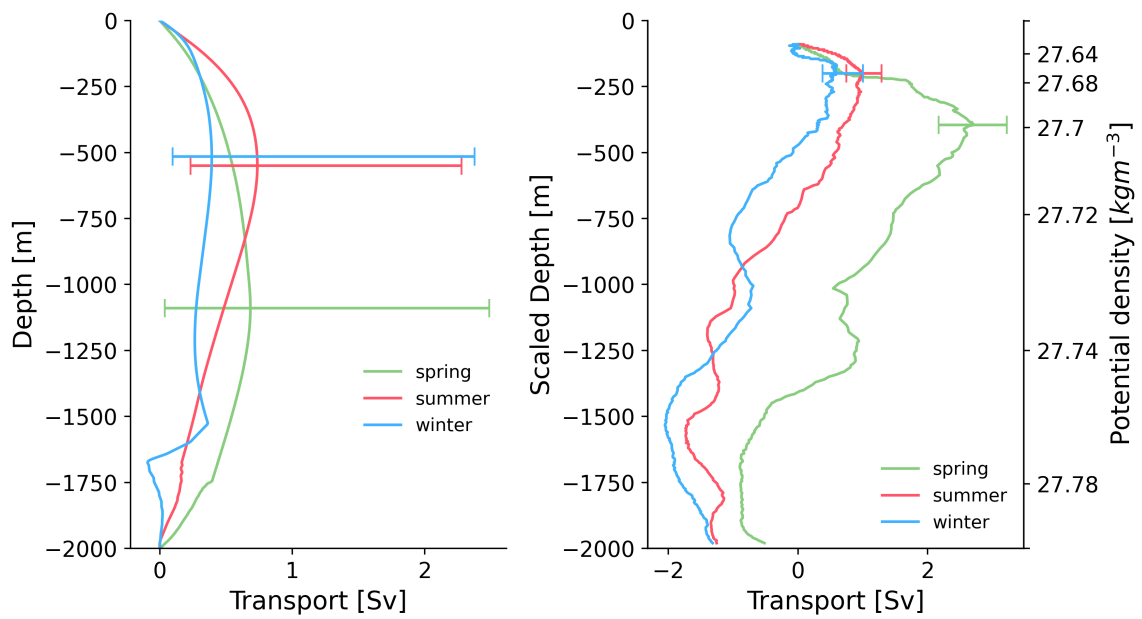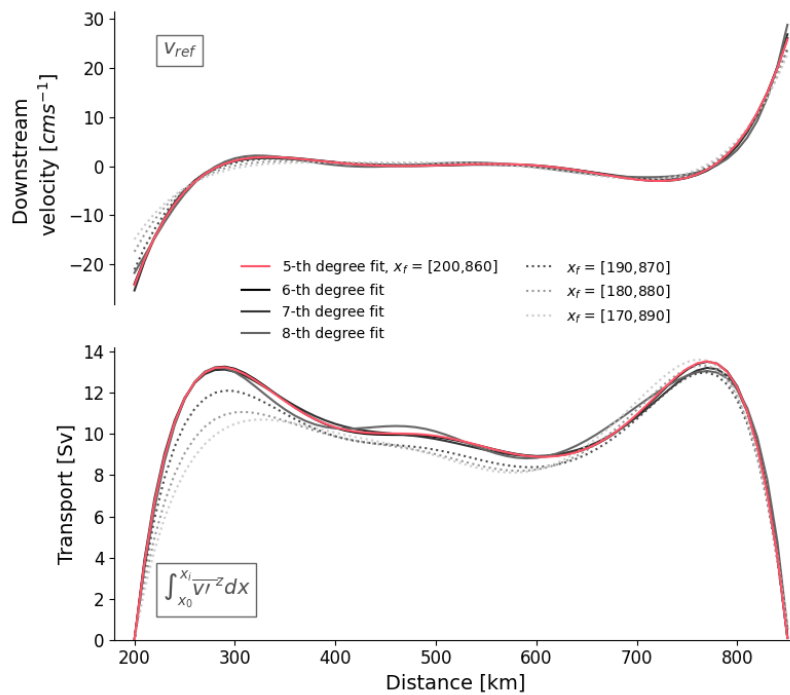

Figure 4: Adjusted seasonal overturning in depth and density space between March 2002 and April 2016

Figure 5: Adjusted seasonal horizontal transport between March 2002 and April 2016

Figure 6: Upper panel: reference velocity with different degrees of the polynomial fit with the same range in x used to fit the data ($x_f = [200, 860]$) (solid lines) and fixed at 5-th degree but with broader x_f (dashed lines), where more data points are included to derive the fits. Lower panel: corresponding mean horizontal overturning without the velocity adjustment.
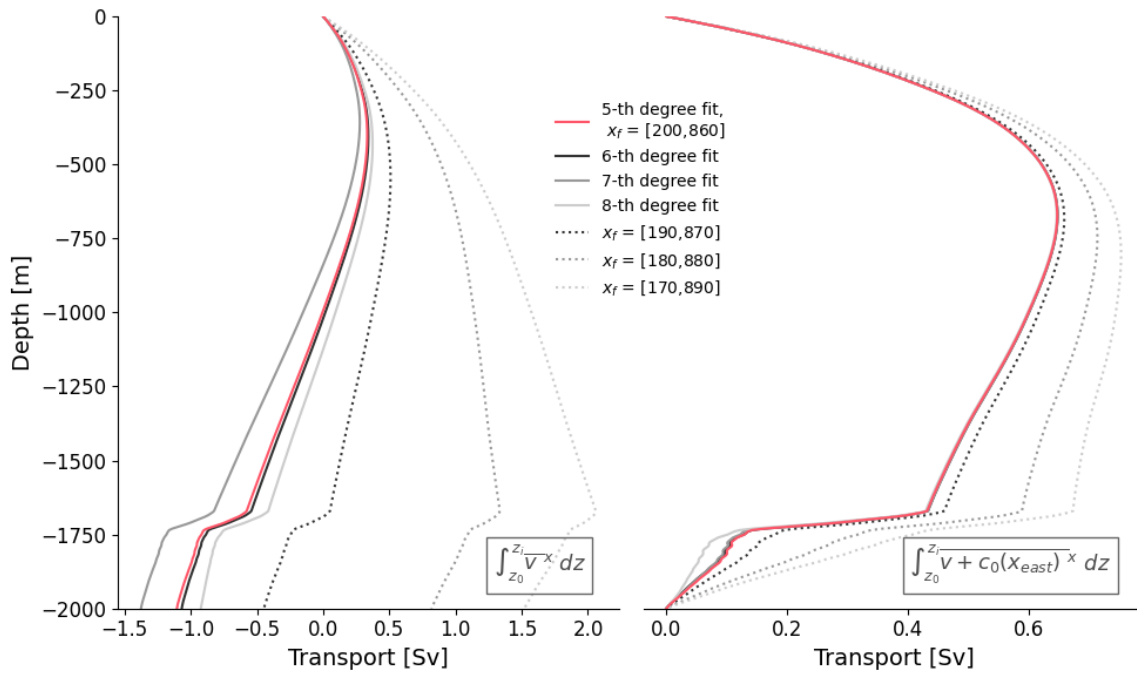
Figure 7: Mean vertical overturning in depth space with (left) and without (right) the velocity adjustment with the same reference velocities used as in fig. 6

Table 1: Cruise Details of hydrographic sections used for a shear estimate

Cruise	Start Date	End Date	Notes
18HU20021129	2002-11-29	2002-12-09	not calibrated
18HU200307_1	2003-07-13	2003-08-04	not calibrated
18HU20040515	2004-05-15	2004-05-30	not calibrated
18HU20050526	2005-05-26	2005-06-07	not calibrated
18HU20060524	2006-05-24	2006-06-08	not calibrated
18HU20070510	2007-05-10	2010-05-27	no quality checks available
18HU20080520	2008-05-20	2008-06-04	no quality checks available
18HU20090517	2009-05-17	2009-06-01	no quality checks available
18HU20110506	2011-05-06	2011-05-29	no quality checks available
06MT20110624	2011-06-24	2011-08-02	quality good
18MF20120601	2012-06-01	2012-06-17	no quality checks available
18HU20130507	2013-05-07	2013-05-28	quality good
06M220130509	2013-05-09	2013-06-20	quality good
18HU20150504	2015-05-04	2015-05-24	no quality checks available

Data availability

I will publish selected code and data on a Github repository, you can soon find here:
https://github.com/katjaschultz/Overturning-in-the-Labrador-Sea.

Eidesstattliche Versicherung

Hiermit versichere ich an Eides statt, dass ich die vorliegende Arbeit im Studiengang M.Sc. Ocean and Climate Physics selbstständig verfasst und keine anderen als die angegebenen Hilfsmittel – insbesondere keine im Quellenverzeichnis nicht benannten Internet-Quellen – benutzt habe. Alle Stellen, die wörtlich oder sinngemäß aus Veröffentlichungen entnommen wurden, sind als solche kenntlich gemacht. Ich versichere weiterhin, dass ich die Arbeit vorher nicht in einem anderen Prüfungsverfahren eingereicht habe und die elektronsiche Version der gedruckten entspricht.

Einer Veröffentlichung der vorliegenden Arbeit in der zuständigen Fachbibliothek des Fachbereichs stimme ich zu.

Hamburg, den   31.07.2024   Unterschrift: